ICAS-98-4,1,1

PREDICTION OF ANTISYMMETRIC BUFFET LOADS ON HORIZONTAL STABILIZERS IN MASSIVELY SEPARATED FLOWS

Saeed Farokhi, CEO and President Aerotech Engineering & Research Corporation Lawrence, KS

Saeid Mirsafian, R&D Engineer, Aerotech Engineering & Research Corporation Lawrence, KS

Tom Sherwood, R&D Engineer, Aerotech Engineering & Research Corporation Lawrence, KS

Mark Ewing, Professor of Aerospace Engineering, University of Kansas, Lawrence, KS

Abstract

A low-cost technique for the prediction of full-scale buffet loads on horizontal stabilizers of general aviation aircraft is described. A 1/13-scale rigid generic wind tunnel model with a t-tail configuration(based on the Beech Super King Air 200) was constructed and tested at the Wichita State University 7x10 ft. subsonic wind tunnel. The test matrix included a dynamic pressure range of 25-45 psf, an angle-of-attack range of -5-20 deg, and a sideslip range of 0-20 deg. The stabilizer was instrumented with differential pressure transducers and strain gages. The measured pressure power spectra and cross-spectral densities were scaled and used to excite a full-scale aeroelastic finite element model which included the tail structure and aft tail cone. The computed horizontal stabilizer rolling moment power spectra are used to determine the number of exceedences (within a known probability) of a specified rolling moment level per a given maneuver(e.g.., stall). Representative pressure, strain gage, and rolling moment power spectra are discussed as is a selected exceedence estimates.

Introduction

The Federal Aviation Administration (FAA) has a continuing program to collect data and develop predictive methods for aircraft flight loads. Some of the most severe and potentially catastrophic flight loads are produced by separated flows. Structural response to the aerodynamic excitation produced by separated flows is defined as buffeting.[1] Buffeting can cause serious controllability problems and in severe cases produce structural failure. The result of control difficulties can be catastrophic if the aircraft is in a near ground flight path such as landing or takeoff. Structural failure, in the extreme, is life-threatening at any flight condition. The potential severity of tail buffet has persuaded the FAA to include buffet loading as a design load criterion for commercial transports. Under Federal Aviation Regulation (FAR) 25-305(e), aircraft manufacturers are required to demonstrate that the cumulative probability of an aircraft encountering dangerous levels of buffet-induced rolling moment is below the prescribed level. The current accepted method of meeting this requirement involves a great deal of full-scale flight testing. This method costs manufacturers a large amount of capital to meet the requirement and allows them no easy recourse should the aircraft not qualify. New methodologies are being considered that would allow the design rolling moment load to be estimated before the full-scale aircraft is constructed. A standardized method would expedite the certification process and enable consistent and repeatable results.

Two major classes of buffet prediction methods are currently in use. The first method is buffet prediction by computational fluid dynamics codes. This method is very computationally intensive, requires an expert user, and is still unproved. An alternate approach is to use experimental data in conjunction with a computational solution of the structural dynamics equations. Experimental/computational methods also have several subdivisions, most notably in the experimental methods employed. The wind tunnel model used for measurement of the unsteady surface pressure can be rigid or flexible. The merits of each type of buffet prediction methodology are summarized in references 2, 3, and 4. This study describes an experimental /computational method to predict anti-symmetric buffeting loads of horizontal stabilizers in massively separated flows. The objective is to predict, within a known probability, the anti-symmetric response. The most obvious benefit is safety. If an aircraft has predictable characteristics in critical flight scenarios, precautionary measures can be taken. If a prediction of undesirable behavior can be performed early in the design process, it can be remedied. Other important benefits of this methodology are reduced design costs and reduced design cycle time.

21st ICAS Congress
13-18 September 1998
Melbourne, Australia

Buffet Prediction Method

Buffeting is governed by the dynamic equilibrium equation (1) given in terms of the generalized coordinate q:[2]

$$M_n \ddot{q}(t) + D_n \dot{q}(t) + \omega_n^2 M_n q_n(t) + F_{D_n}(q_1(t)\ldots\dot{q}_N(t)) + \\ + F_{K_n}(q_1(t)\ldots q_N(t)) = P_n(t) \qquad (1)$$

where the first three terms represent the generalized mass, structural damping, and structural stiffness respectively. The following two terms are the motion-dependent aerodynamic damping and the motion-dependent aerodynamic stiffness. The term on the right-hand-side is the motion-independent aerodynamic force(buffet pressure excitation).[2]

Although there are several approaches to solving equation (1), a rigid body method for buffet prediction was chosen due to its relatively low cost and experimental simplicity. The prediction methodology can be divided into two distinct tasks: (1) experimental acquisition of unsteady pressures on the tail of a rigid model, and (2) prediction of the aeroelastic results based on the buffet forcing function as defined by the first task. The prediction of tail buffet using this methodology can be best summarized in the flowchart illustrated in Figure 1.[5]

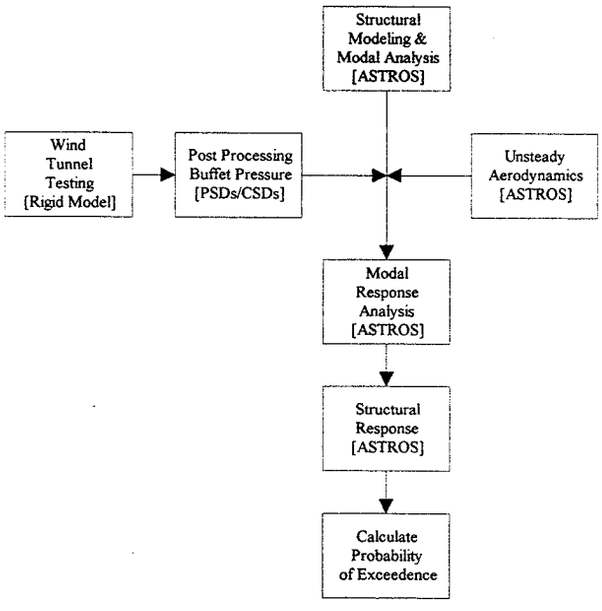

FIGURE 1 - Schematic Representation of Buffet Prediction

Experimental Methods

Test Facility

The experimental testing was performed at the National Institute for Aviation Research (NIAR) facilities in Wichita, Kansas. The Walter H. Beech Memorial Wind Tunnel which has a 7- by 10-foot test section was used. Model support was achieved by a sting which could be used to vary the model angle-of-attack from -5-20 deg. The sting was mounted on a rotary table which allowed the sideslip angle to be adjusted. The test matrix is given in Table 1. These dynamic pressures represent a Reynolds number range of 9.2×10^5/ft to 1.2×10^6/ft.

Dynamic Pressure (psf): 25, 35, 45
Angle of Attack (degrees): -5, 0, 5, 10, 15, 20
Heading Angle (degrees): 0, -10, -20

Table 1 - Test Matrix

Model Design

The model used for the tests was a rigid 1/13-scale generic t-tail model based on the Beech Super King Air 200 and it can be seen in Figure 2. The model consists of three major sections: the wing, fuselage, and tail. The dimensions for the model were primarily driven by the load limitations of the sting mount.

The wing is formed by a plywood/fiberglass skin coating over a styrofoam core which has an aluminum spar running the entire span for added rigidity. The fuselage consists of two halves bolted together. A 1.25-inch thick aluminum plate runs along the bottom fuselage section and allows for the attachment of the wind as well as the sting mount. The vertical tail structure is machined aluminum. The stabilizer is of a clam-shell design with the two halves bolted together. This allows for access to the pressure transducers.

The stabilizer was made about six percent thicker than on the full-scale aircraft to allow for room for mounting the pressure transducers. This construction technique was deemed sufficient because extreme accuracy in the shape and thickness of the stabilizer does not play a significant role in this study.

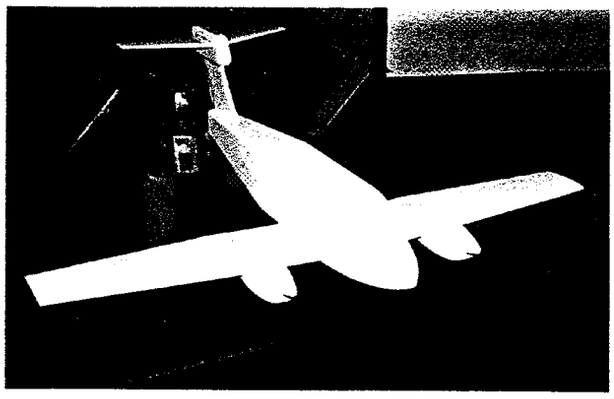

FIGURE 2 - Wind Tunnel Model of Beech Super King Air 200

Instrumentation

The pressure transducers used for measuring the horizontal tail pressures were Kulite LQ-1-200-5D (Range: 5 PSID). These transducers have a high natural frequency of over 70 kHz and have a linear response in the region of interest for the present tests. Twelve transducers were mounted in the center of the stabilizer at the locations shown in Figure 3. Small holes were drilled in the stabilizer skin to vent the transducers to the upper and lower surfaces. The numbers in Figure 3 represent the channel numbers referred to later in this report.

To remove the signal which is attributable to the free stream signal, the free stream pressure had to be recorded. A Kulite LQ-125-5SG pressure transducer with the following characteristics: 0-5 psi measuring range, non-linearity and hysteresis +/- 0.5%, and a natural frequency of 70-350 kHz was used for this purpose. It was mounted at the forward end of the test section out of the tunnel boundary layer and out of the influence of the model.

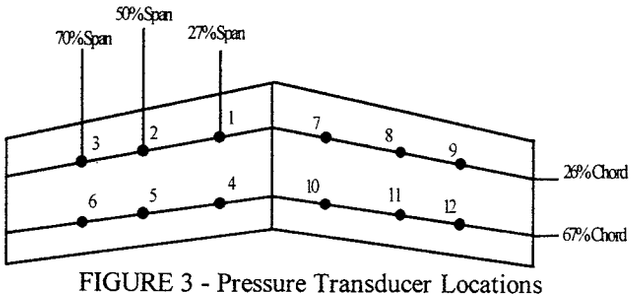

FIGURE 3 - Pressure Transducer Locations

The strain gages used were Omega KFG-10-120-C1-11L1M2R pre-wired gages. They were mounted as close to the root of the horizontal tail as possible in the configuration shown in Figure 4. The 1/2-bridge configuration, unlike the full-bridge, allows for the resolution of both bending and torsional loads. The 1/2-bridge configuration also eliminates the need for temperature compensation and has a larger output signal than a 1/4-bridge setup. The strain gage configuration as shown in Figure 4 have the following characteristics (for bending strain): 10 μV/με output given a 10 V excitation, with a sensitivity of 1.0 mV/V at 1000 με.[6]

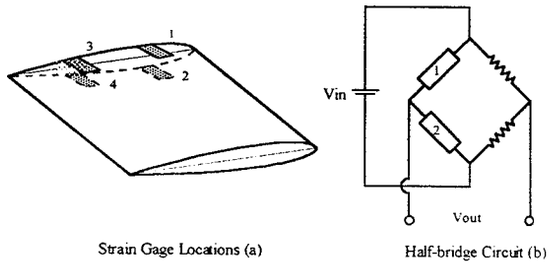

FIGURE 4 - Strain Gage Locations and Strain Gage Circuitry

Data Acquisition

A schematic of the data acquisition procedure can be seen in Figure 5. AC coupling was enabled during data acquisition to remove the DC component of the signal. The AC coupling was accomplished using a 2200 System from Vishay. In total, seventeen 2210 signal conditioning amplifier units were used for the pressure transducer and strain gage channels. This unit also provided the signal amplification and low pass filtering functions. The low-pass filter used was a four-pole Bessel with a cutoff frequency of 1000 Hz. Low-pass filtering is required to prevent aliasing (the process of high frequency data 'folding over' into the lower frequency range) in the data.[6,7]

HP-44730A (4-channel/card) simultaneous track-and-hold cards were used in this experiment. Although there is only one analog-to-digital converter in the HP-3835, these cards allowed the simultaneous acquisition of all of the transducers by providing a buffer. This prevents a lag between data points which, in turn, prevents the data from being time skewed (accurately preserving the phase data).

To set the amplification for both pressure transducer and strain gage data, a representative signal was recorded using no amplification, and then the amplification was set to a value to ensure the maximum amount of resolution of the signal without exceeding the input range of the A/D board.

At each point in the test matrix listed above, 51,200 data points per channel (51,200x17=870,400

total) were recorded at a sampling frequency of 4000 Hz.

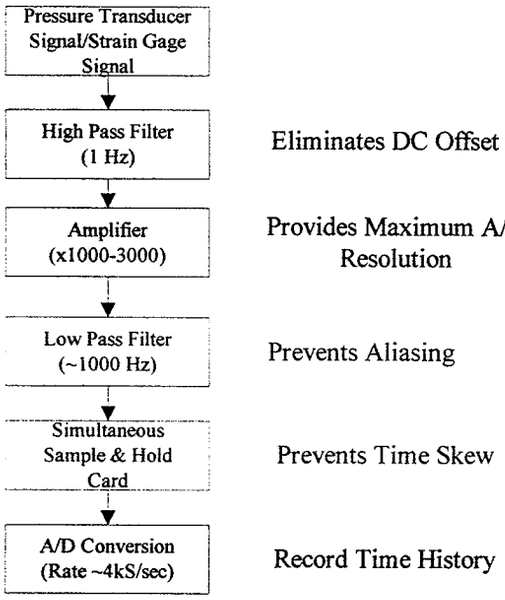

FIGURE 5 - Schematic of Signal Conditioning and Raw Data Recording

Data Postprocessing and Analysis

The data postprocessing begins where the last box in Figure 5 ends. There were two goals of the postprocessing data analysis. The first was to convert the time series pressure data obtained from the wind tunnel to a format compatible with the computational tail buffet prediction, and the second was to convert the time series strain gage data into a format compatible with the estimation of the power spectra of the horizontal tail root bending moment as check of the validity of the pressure measurements.

Pressure Data

The most efficient and popular method for estimating the power spectral densities of time data is the Fast Fourier Transform. The expressions for the one-sided power spectra and the cross-spectral density estimations are given by equations (2) and (3) respectively.

$$\hat{G}_{xx}(f)=\frac{2}{\eta_d T}\sum_{k=1}^{\eta_d}\left|X_k(f,T)\right|^2 \qquad (2)$$

$$\hat{G}_{xy}(f)=\frac{2}{\eta_d T}\sum_{k=1}^{\eta_d}X_k{}^*(f,T)Y_k(f,T) \qquad (3)$$

To reduce the error associated with the inherent windowing of the data(rectangular windowing), the Hanning window was applied to the data prior to the calculation of the spectra. The noise floor was then subtracted from these results. The power spectrum of the measured pressures also included the contribution of the free-stream signal which was not desired. To eliminate this portion of the signal, the coherence between the free-stream signal and the stabilizer signals were determined using equation (4). The values were then corrected using the relation given in equation (5).

$$\hat{\gamma}_{xy}{}^2(f)=\frac{\left|\hat{G}xy(f)\right|^2}{\hat{G}xx(f)\,\hat{G}yy(f)} \qquad (4)$$

$$\hat{G}xx(f)=\left[1-\hat{\gamma}_{xf}{}^2(f)\right]\hat{G}xx^*(f) \qquad (5)$$

While not completely eliminated, the influence of strongly coherent signals, such as the blade frequency of the wind-tunnel propeller and the associated higher harmonics, are greatly reduced through the application of equation (5).

To apply the PSD and CSD pressure data to a full-scale finite element model scaling laws needed to be applied. Equations (6) and (7) give the scaling laws used in this study(a refers to aircraft scale and m refers to model scale):

$$P_a=[(l_a/l_m)(\rho_a/\rho_m)^2(V_a/V_m)^3]P_m \qquad (6)$$

$$f_a=[(V_a/V_m)/(l_a/l_m)]f_m \qquad (7)$$

These scaling laws are taken directly from reference 3. To check the validity, similar validation plots to those found in reference 3 were prepared. These can be seen in Figures 6 and 7. The are in agreement with the results given in reference 3 and the scaling laws are assumed to be valid. Figures 8a-c show typical variations of pressure PSD values with angle-of-attack. Since no significant flow separation exists for the conditions in Figure 8a it will not be compared with Figures 8b and 8c. The frequency corresponding to the peak level of PSD shifts to a higher value with increasing angle-of-attack. Because this study only included two points within this highly separated range, it is difficult to draw any clear conclusions from this trend.

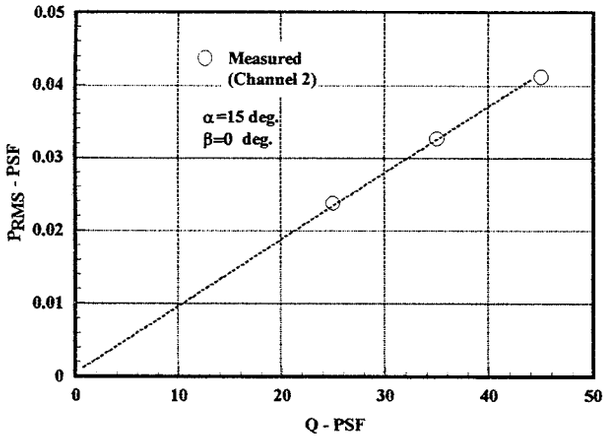

FIGURE 6 - Validation Check of RMS Buffet Pressure Scaling (1/13th Scale Wind Tunnel Model)

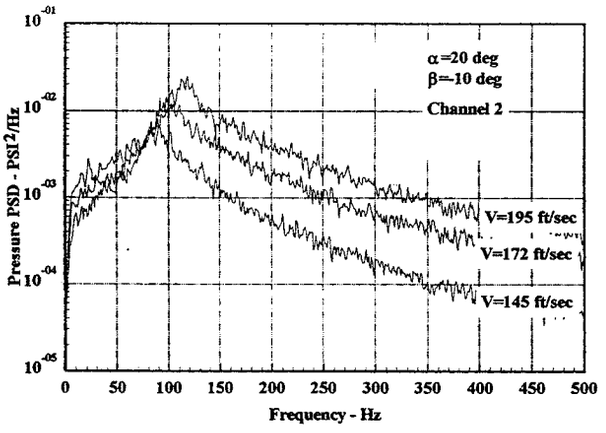

FIGURE 7 - Validation of Buffet Pressure Scaling Characteristics with Airspeed

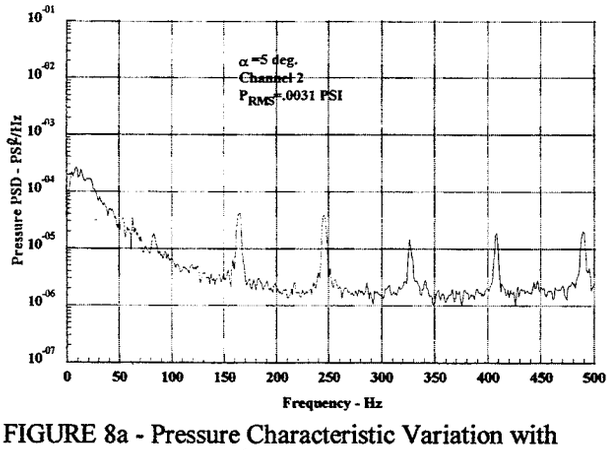

FIGURE 8a - Pressure Characteristic Variation with Angle-of-Attack (1/13th Scale Wind Tunnel Model, Q=45 PSF)

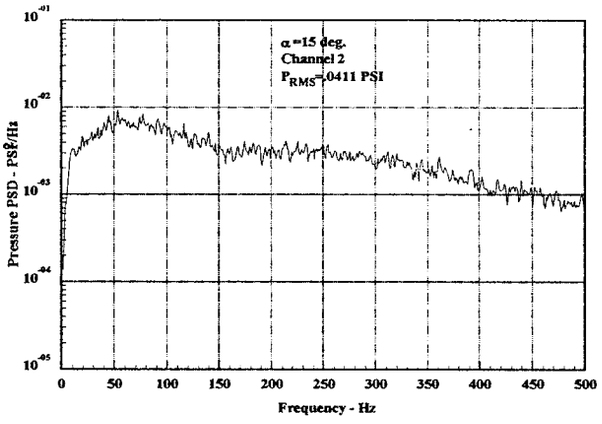

FIGURE 8b - Pressure Characteristic Variation with Angle-of-Attack (1/13th Scale Wind Tunnel Model, Q=45 PSF)

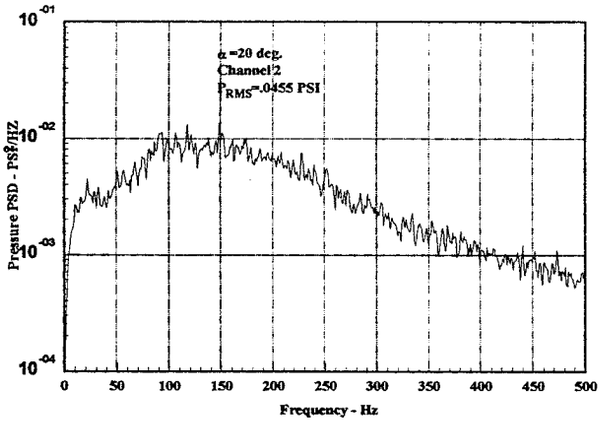

FIGURE 8c - Pressure Characteristic Variation with Angle-of-Attack (1/13th Scale Wind Tunnel Model, Q=45 PSF)

Strain Gage Data

The strain gage data was analyzed in a manner similar to the pressure data, except that the removal of the coherent data was eliminated. The strain gage data was used to provide a check for the accuracy of the pressure data. To determine this, the pressure data was used in conjunction with a simple finite element model of one side of the horizontal stabilizer. The PSD for the bending moment were calculated at the same locations as the strain gages. The results indicated reasonable agreement between the measured root bending moment via the strain gages and those predicted by the measured buffet pressures and finite element model.

Finite Element Analysis

Finite Element Model

The finite element model used in this study can be seen in Figure 9. It was produced using the MSC/XL

software package. Table 2 lists the major dimensions for the model shown in Figure 9, while Table 3 lists the separate element types used for the aircraft structure. The dimensions of the structural components were estimated using data and drawings from reference 8. The model is restrained in all six degrees-of-freedom at the grid points which define the forward ring frame. The aft fuselage(tail cone) structure was included in the model primarily for its torsional characteristics. Table 4 lists the first nine natural frequencies along with their associated mode shapes. Note that the frequencies referred to here are full-scale frequencies. The appropriated scaling laws are given in the following section. This analysis was limited to these nine frequencies due to the available computational resources. However, the first few modes play the dominant role in the horizontal stabilizer rolling moment due to buffet, therefore this number of modes was deemed sufficient. Of these nine modes, five are localized in the forward bulkhead which lies inside the ring frame which the front spar of the vertical tail attaches. Although these modes either will not exist in an actual aircraft, or if they do, they will be insignificant, they were included for computational ease. Figures 10-13 show the four most important modes in this analysis. The first bending mode occurs at 12.7 Hz. Since the problem at hand is anti-symmetrical in nature this is an important mode. This mode causes the aft spar of the vertical tail to move in a lateral motion while the front spar remains relatively fixed. Mode two occurs at 15 Hz. This mode is similar to mode six which occurs at 26.2 Hz. They are both symmetrical flapping modes. During mode two, the vertical moves forward and aft along with the horizontal stabilizer flapping motion. As the vertical tail structure reaches its furthest point forward, the tips of the horizontal stabilizer are at their highest point. The reverse is true for mode 6. As the vertical tail structure reaches its furthest point forward, the horizontal stabilizer tips bend downward and reach their lowest point. The final mode of interest is the secondary bending mode which occurs at a frequency of 24.2 Hz. In addition to its bending, it imparts a torsional load to the fuselage structure.

CHARACTERISTIC	VALUE
Tail Span	121 inches
Root Chord	60 inches
Tip Chord	30 inches
Root Depth	6 inches
Tip Depth	3 inches
Front Spar	15% Chord
Rear Spar	Elevator Hinge Line

Table 2 - Geometric Values Used for FEM

COMPONENT	ELEMENT	PROPERTIES
Skin	cquad4/ctria3	0.032 in. thick
Longeron	cbar	1.25"x1/8"x2" I-Beam
Ring Frame	CBAR	1.25"x1/8"x2" I-Beam
Ribs(web)	CSHEAR	0.1 in. thick
Spar(web)	CSHEAR	0.1 in. thick
Bulkheads	CQUAD4	0.1 in. thick
Rib(flange)	CROD	0.1 sq. in. area
Spar(flange)	CBAR	1.25"x1/8" Beam

Table 3 - Finite Element Types Used in the Analysis

Mode Number/Frequency	Type
1 12.7 Hz	First Bending Mode
2 15.0 Hz	First 'Flapping' Mode
3 23.1 Hz	Local Forward Bulkhead
4 24.2 Hz	Second Bending Mode
5 25.9 Hz	Local Forward Bulkhead
6 26.2 Hz	Second 'Flapping' Mode
7 41.3 Hz	Local Forward Bulkhead
8 46.4 Hz	Local Forward Bulkhead
9 49.9 Hz	Local Forward Bulkhead

Table 4 - Natural Frequency and Modes

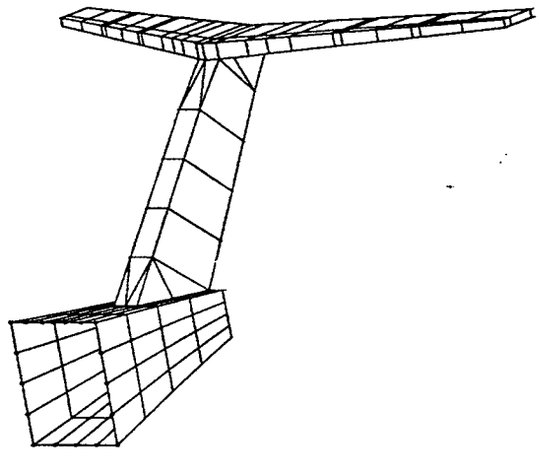

FIGURE 9 - Finite Element Model of Beech Super King Air 200 Aft Tail Cone and Tail Structure

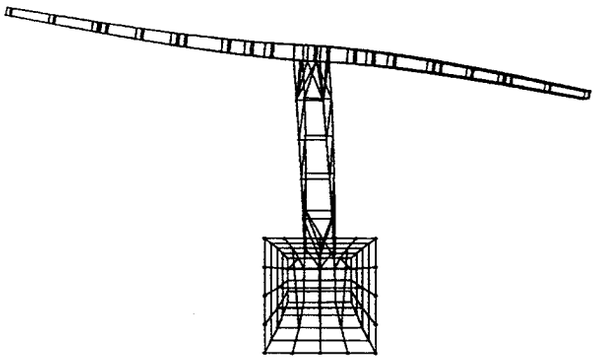

FIGURE 10 - Mode 1 of Tail Structure (f_n=12.7 Hz)

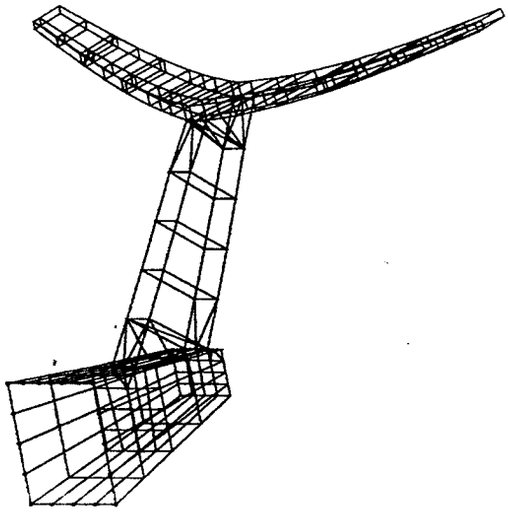

FIGURE 11 - Mode 2 of Tail Structure (f_n=15.0 Hz)

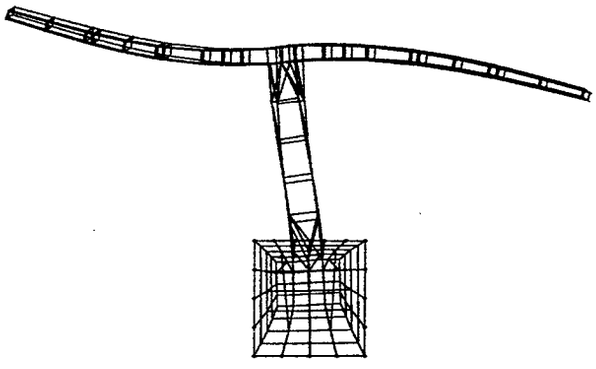

FIGURE 12 - Mode 4 of Tail Structure (f_n=24.2 Hz)

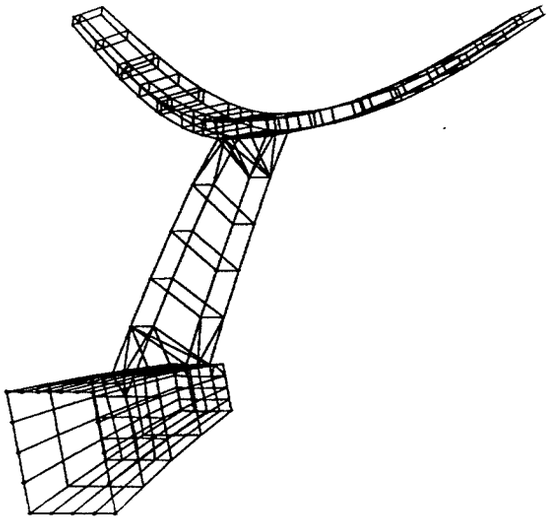

FIGURE 13 - Mode 6 of Tail Structure (f_n=26.2 Hz)

Finite Element Analysis Procedure

ASTROS (Automated STRuctural Optimization System) finite element software was used for the finite element analysis. This program is a multidisciplinary finite element-based procedure for the design and analysis of aerospace structures.[9] It is public domain program with proven capabilities paralleling those of the widely used NASTRAN. ASTROS is written in a flexible high-level language, MAPOL (Matrix Analysis Problem Oriented Language). Although the program does not directly support buffet analysis, ASTROS can be used for buffet analysis by modifying the standard MAPOL sequence. All of the terms on the left-hand-side of equation (1) were determined using ASTROS. As mentioned previously, linear modal analysis was performed to determine the natural frequencies and mode shapes of the system, and this determines the first three terms in equation (1). Since the buffet pressure excitation, P_n, was determined experimentally in the wind tunnel, only the motion-dependent aerodynamic and stiffness terms remain to be solved.

The ASTROS flutter, gust, and blast analyses solution sequences include the aerodynamic stiffness and damping terms of equation (1). These terms are computed by use of the doublet lattice method which is recognized as a standard in the aerospace industry. The aerodynamic model was created using aerodynamic panel elements(CAERO1). For this study, only the horizontal stabilizer was modeled for these terms.

There are two differences between the present problem and the ASTROS gust analysis solution sequence: (1) the right-hand side of equation (1) is different, and (2) gust analysis in ASTROS is treated as

a frequency response analysis, not a random response analysis. The present buffet problem was solved using a multi-step approach.

The first step was to determine the modal complex frequency response matrix, [H(ω)]. This matrix can be computed at each frequency of interest by replacing the gust analysis right-hand side with the identity matrix. The resulting response matrix is [H(ω)].

Step two is to perform the following matrix multiplication to determine the modal buffet pressures:

$$[S_x(\omega)]=[\phi]^T[S(\omega)][\phi] \quad (8)$$

where [S(ω)] is a matrix of forces corresponding to the pressures measured in the wind tunnel. To determine this matrix the pressures were first scaled to full-scale using the equations (4) and (5) and then multiplied by the area which they act.

The third step is to compute the modal response PSD matrix, [S(ω)]. This matrix multiplication is given by equation (9).

$$[S(\omega)]=[H(-\omega)][S_x(\omega)][H(\omega)]^T \quad (9)$$

The fourth step involves using ASTROS to calculate the structural responses, $[N_y]$ due to unit modal displacements. This requires the MAPOL sequence to be modified in a similar manner to the first step in this process. The terms in the row matrix $[N_y]$ are the structural responses due to unit modal displacements. For example, if the desired output is the PSD of the axial force in a bar element, N_{y11} represents the axial force due to $q_1=1$ and $q_2=q_3\ldots q_{(\#\ modes)}=0$.

The fifth step is to solve for the structural responses, $[S_y(\omega)]$ using equation (10).

$$[S_y(\omega)]=[N_y][S(\omega)][N_y]^T \quad (10)$$

The complex structural responses found using equation (10) can be used to determine a variety of structural responses. What is of interest to this study is the rolling moment generated on the horizontal stabilizer. This was determined by averaging the forces as shown in Figure 14. These are the axial forces in the CBAR elements which model the attachment of the vertical tail to the horizontal stabilizer. Since these values are complex, the phase information from the wind tunnel pressures are preserved and by taking the difference an overall rolling moment can be generated.

$$[(F1+F2)-(F3+F4)]d \quad (11)$$

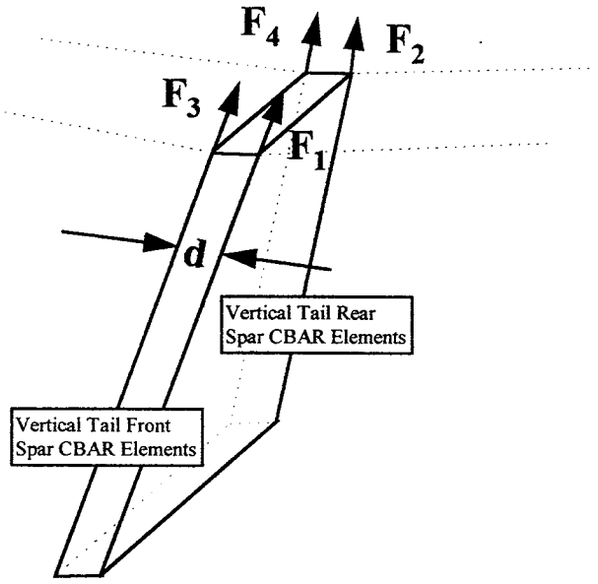

FIGURE 14- Axial Force Components Used for Rolling Moment Computation

Figures 15a-f show a representative series of horizontal stabilizer rolling moments generated in this manner. Although the data extends to nearly 80 Hz(full-scale), little happened past 50 Hz, therefore only 0-50 Hz was plotted. Figures 15a-d indicate very little buffet induced rolling moment as to be expected from the combination of low dynamic pressure angle-of-attach and side-slip angle. Figures 15e-f indicate much higher rolling moments than the other four cases as is expected as the highly separated flow field at these conditions impinges on the stabilizer.. In all cases, the first two modes have the highest response indicating their importance to the buffet-induced rolling moment phenomenon.

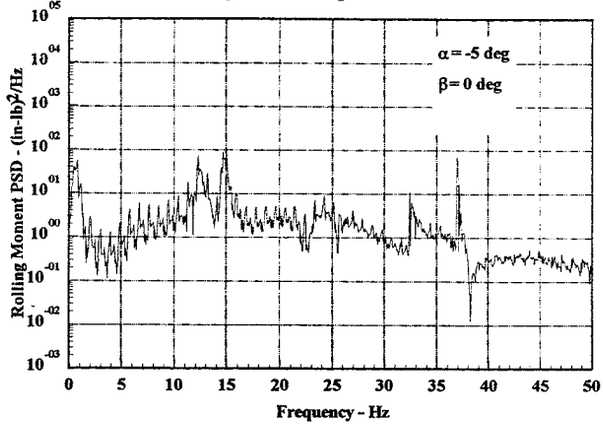

FIGURE 15a - PSD of Predicted Rolling Moment (Q = 25 PSF)

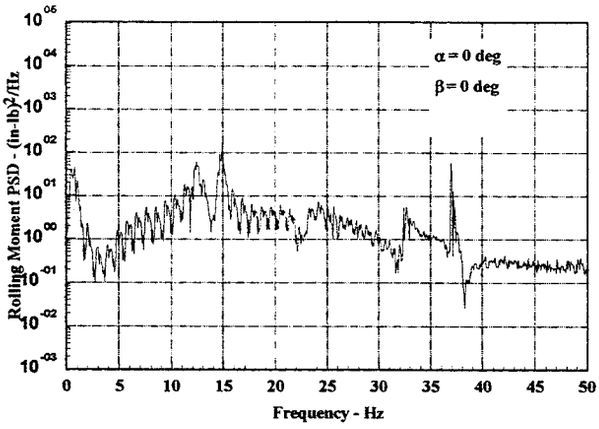

FIGURE 15b - PSD of Predicted Rolling Moment (Q = 25 PSF)

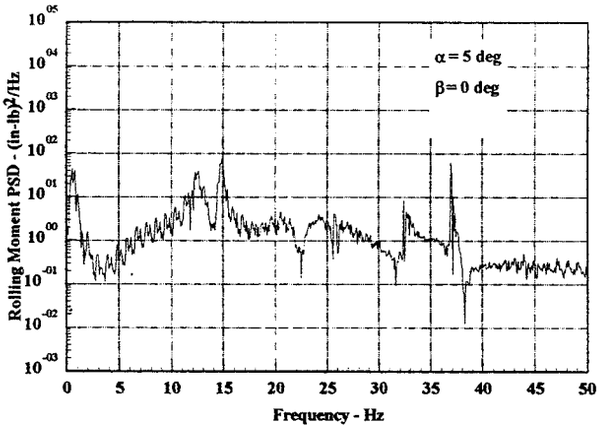

FIGURE 15c - PSD of Predicted Rolling Moment (Q = 25 PSF)

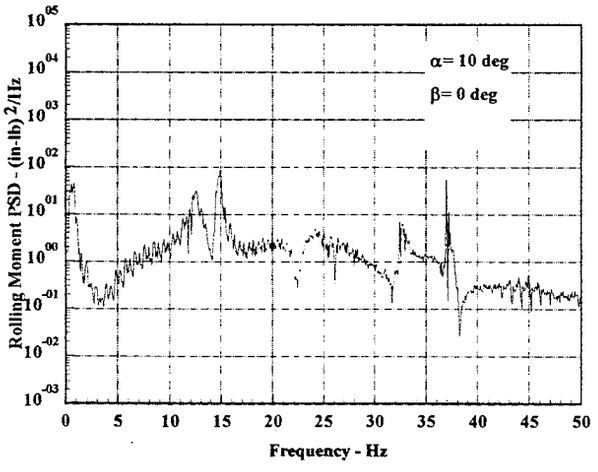

FIGURE 15d - PSD of Predicted Rolling Moment (Q = 25 PSF)

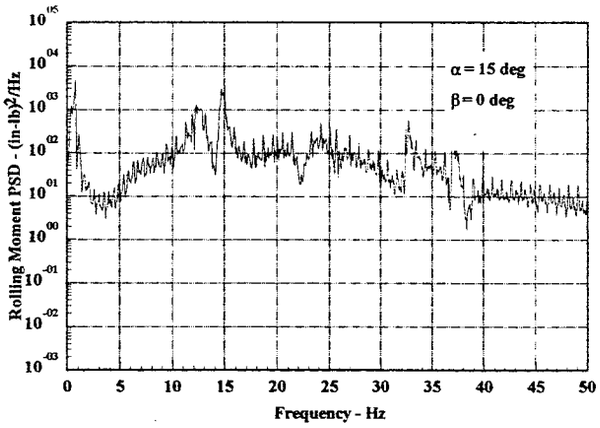

FIGURE 15e - PSD of Predicted Rolling Moment (Q = 25 PSF)

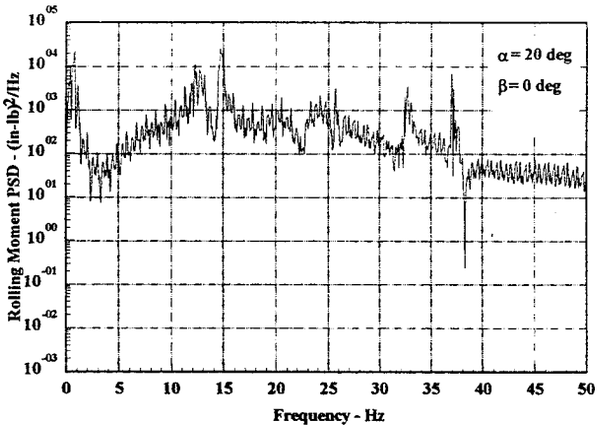

Figure 15f - PSD of Predicted Rolling Moment (Q = 25 PSF)

The final step in the design procedure is to determine the number of exceedences of a given loading level (in this case rolling moment on the horizontal stabilizer) that occur for a specific flight history as indicated in Figure 16. Equation (12) shows the method used.

$$N(R.M.) = \sum_{k=1}^{X} f_k \sum_{i=1}^{I} P_{i,k}(R.M.)t_i \qquad (12)$$

The $P_{i,k}$ term in equation (12) represents the probability that a given peak of the structural response PSD will exceed a given level. This is given by the relation shown in equation (13). This represents the Rayleigh distribution which applies to the peak values in the PSD of random responses.[10]

$$P_{i,k}(R.M.) = \int_{\frac{R.M.}{\sigma_{i,k}}}^{\infty} \frac{R.M.}{\sigma_{i,k}^2} e^{-R.M.^2/2\sigma_{i,k}^2} d(R.M.) \qquad (13)$$

The variance in equation (13) is given by:

$$\sigma^2_{i,k} = -\frac{E_{j,j}(f_k) f_k \pi}{4\xi_k} \qquad (14)$$

$E_{j,j}(f_k)$ is the PSD of the rolling moment calculated using equation (11) and ξ_k is the structural damping which is assumed to be 0.03 for this study.
The final step is to calculate several values using equation (12) and plot the results.

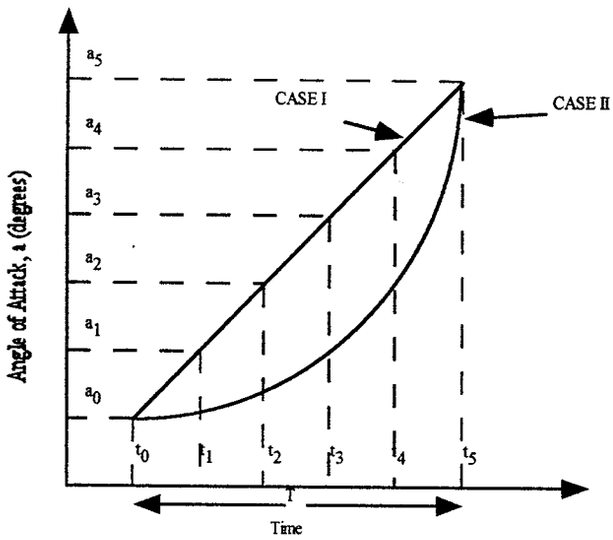

FIGURE 16 - Definition of a Stall Event

The data given in Figures 15a-f were used in conjunction with equations (12)-(14) to determine a predicted design curve for the number of exceedences for a given stall event. This figure was made for methodology demonstration only. The stall event was assumed to occur in a linear fashion with the aircraft holding each one of the six loading conditions(there are six angle-of-attack data points) for two seconds. As expected from equation (13), the curve drops rapidly with increasing specified rolling moment levels until it nearly reaches zero by a rolling moment of 5000 in-lbs.

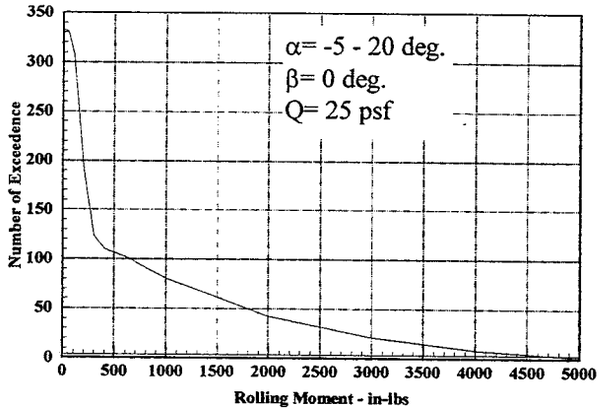

FIGURE 17 - Prediction of Number of Exceedences for a Given Stall Event

Summary

Based on rigid model wind tunnel pressure measurements and an aeroelastic, full-scale finite element model, a design methodology for the rapid and low-cost assessment of the rolling moment loads due to asymmetric horizontal stabilizer buffeting has been demonstrated. Now that the feasibility of the process has been demonstrated, the validity of the approach needs to be determined. This would be accomplished by applying this methodology to an actual aircraft and follow up the predictions with flight tests to confirm the results.

Acknowledgments

The authors would like to extend their appreciation to Mr. Terry Barnes of the Federal Aviation Administration for his technical advice throughout the duration of this research and to Mr. Tom DeFiore, also of the FAA for his project oversight.

References

1. Triplett, W. E., "Pressure Measurements on Twin Vertical Tails in Buffeting Flow," *Journal of Aircraft*, Vol. 20, No. 11, November 1983, pp. 920-925.
2. 2. Mauk, C.S., "Methods of Stochastic Modeling of Antisymmetric Buffet Loads on Horizontal Stabilizers in Mssively Separated Flows," Aerotech Technical Report AER TR93-052, May 5, 1993.
3. Ferman, M. A., Patel, S. R., Zimmerman, N. H., and Gerstenkorn, G., "A Unified Approach to Buffet Response of Fighter Aircraft Empennage," AGARD CP-483, 1990.
4. 4. Butler, G. F., and Jones, J. G., "The Prediction of Buffeting Response in Flight from Wind-Tunnel Measurements on Models of Conventional

Construction," *Aeronautical Journal*, Aug./Sept. 1984.

5. Farokhi, S., Mauk C. S., and Locke, J. E., "Stochastic Modeling of Antisymmetric Buffet Loads on Horizontal Stabilizers in Massively Separated Flows," U.S. DOT (FAA) Final Report March 1996.
6. Bendat, J. S., and Piersol, A. G., Random Data: Analysis and Measurement Procedures, John Wiley & Sons, New York, 1986.
7. Bendat, J. S., and Piersol, A. G., Engineering Applications of Correlation and Spectral Analysis, John Wiley & Sons, New York, 1993.
8. Taylor, J.W.R., Jane's All The World Aircraft, Jane's Publishing Company, London.
9. Neill, D.J., and Herendeen, D.L., ASTROS Enhancements: Volume I - ASTROS User's Manual, WL-TR-93-3025, March 1993.
10. Wirsching, H..P., Paez, L. T., and Ortiz, K., Random Vibrations: Theory and Practice, John Wiley & Sons, New York, 1995.